Journal of Alloys and Compounds 509 (2011) 2597–2601

Contents lists available at ScienceDirect

Journal of Alloys and Compounds

journal homepage: www.elsevier.com/locate/jallcom

Structural, electrical and piezoelectric properties of nanocrystalline tin-substituted barium titanate ceramics

K. Chandramani Singh [a,*], A.K. Nath [a], Radhapiyari Laishram [b], O.P. Thakur [b]

[a] Department of Physics, Sri Venkateswara College, University of Delhi, New Delhi 110021, India
[b] Solid State Physics Laboratory, Lucknow Road, Timarpur, Delhi 110054, India

ARTICLE INFO

Article history:
Received 2 August 2010
Received in revised form
13 November 2010
Accepted 15 November 2010
Available online 23 November 2010

Keywords:
Ceramics
Sintering
Hysteresis
Ferroelectricity

ABSTRACT

Barium stannate titanate $Ba(Ti_{1-x}Sn_x)O_3$ ceramics with $x = 0$, 0.025, 0.045 and 0.065 were synthesized using nanocrystalline powders of about 86-nm particle size. The effects of the increasing Sn content on the dielectric, polarization, strain and piezoelectric behavior of the ceramics were studied. In the range of composition studied, an increase in Sn concentration causes the Curie temperature (T_c) to decrease from 115 °C to 45 °C and the phase transition to become more diffuse. Increasing Sn content in the ceramics produces decrease in remnant polarization (P_r) from 5.2 μC/cm² to 0.3 μC/cm² and coercive field (E_c) from 4.6 kV/cm to 0.8 kV/cm. The unipolar strain level of ~0.097% for $x = 0$ gradually decreases to ~0.027% as the value of x increases to 0.065. The electromechanical coupling factor k_p and the piezoelectric charge constant d_{33} also show gradual decline from 41.2% to 19.3% and 183 pC/N to 4 pC/N respectively as the Sn content in the ceramics increases.

© 2010 Elsevier B.V. All rights reserved.

1. Introduction

Barium titanate $BaTiO_3$ (BT) is one of the most widely studied lead-free ferroelectric ceramics due to its excellent properties, high dielectric constant [1,2] and low loss characteristics [3]. At the Curie temperature of 120 °C, the crystal structure of BT changes from tetragonal to cubic accompanied by a sharp peak in the relative permittivity. By adding suitable dopants to BT, interesting characteristics for various applications can be obtained [4–6]. The electrical and dielectric properties of BT can be modified by doping with various isovalent cations on both A(Ba) and B(Ti) sites [7–9]. The A site dopants such as Sr^{2+} are effective in displacing or shifting the Curie temperature but have little effect on dielectric maximum [7]. However the addition of cations on the B site such as Zr^{4+} has significant effect on dielectric maximum [8,9]. The piezoelectric properties of $(Ba_{0.95}Ca_{0.05})(Ti_{1-x}Zr_x)O_3$ ceramics sysnthesized by solid state reaction method are reported to be enhanced at an optimim Zr content of $x = 4$ at.% [10]. Among the modified BT compositions, the barium stannate titanate $Ba(Ti_{1-x}Sn_x)O_3$ (BTS) system in which Sn^{4+} replaces Ti^{4+}, has attracted considerable attention due to their physical mechanism of diffuse-type phase transition [11–13]. Barium stannate titanate is a binary solid solution system composed of ferroelectric barium titanate and non-ferroelectric barium stannate, and both of the two end compositions are of perovskite structure. The strong broadening of permittivity maximum observed at the ferroelectric phase transition in BTS (diffuse phase transition) with increasing amount of Sn was explained on the assumption that local crystal regions have different ferroelectric phase transition temperatures due to composition fluctuations, namely, the distribution of the local Curie temperature (composition fluctuation model) [14]. Isupov [15] explained some problems of ferroelectrics with diffuse phase transitions in view of the polar regions. The BTS ceramics may find applications for various purposes because the Curie temperature (T_c) can be widely shifted by changing the Sn content [16]. Cai et al. [17] observed decrease in remanent polarization, and enhancement in the diffuseness of phase transiton and coercive field of BTS ceramics as the Sn content increases from 0.10 to 0.20. The effect of lanthanum (La) substitution on dielectric behavior of $BaTi_{0.85}Sn_{0.15}O_3$ ceramics has also been studied [18]. Effects of dysprosium (Dy) amphoteric doping on the structural, dielectric and electric properties of BTS ceramics have also been studied [19]. A short time spark plasma sintering method has been used for synthesis of high density (99%) $Ba(Ti_{0.87}Sn_{0.13})O_3$ ceramic which exhibits high relative dielectric constant of 5680 and low dissipation factor ($\tan\delta = 0.009$) at Curie temperature of 57 °C, good tunability and ferroelectric properties [20]. The BTS system attracted many research interests recently due to its abnormal dielectric properties and strong dielectric nonlinearity for the application in tunable microwave electronics. One useful property of BTS system is the unusual strain curve of Ba $(Sn_{0.15}Ti_{0.85})O_3$, in which the domain reorientation occurs only at low fields, and there is then a long

* Corresponding author. Tel.: +91 11 27457625; fax: +91 11 24118535.
E-mail address: kongbam@gmail.com (K.C. Singh).

0925-8388/$ – see front matter © 2010 Elsevier B.V. All rights reserved.
doi:10.1016/j.jallcom.2010.11.106

linear range at higher fields; that is, the coercive field is unusually small [21]. To fully understand this property, which is of great importance in fabricating actuators, it is desirable to investigate in detail the ferroelectric and piezoelectric properties of BTS system. Moreover, the BTS system is particulary intriguing since it contains no Pb ions, an essential feature as environmental concerns grow in the future.

On the other hand, there are reports of great improvement on the physical, electrical and piezoelectric properties of BT ceramics synthesized from nanopowders [22,23]. Dielectric constant is also reported to be strongly dependent on the particle size [24]. It is reported that ferroelectricity in electroceramics decreases with decreasing particle size and disappears below certain critical size [25]. The increase of Sr content in $Ba_{(1-x)}Sr_xTiO_3$ ceramics synthesized from nanopowders causes the inhibition of grain growth and downward shift of Curie temperature (T_c) [26]. It is also reported that the nano-crystalline $Ba_{0.5}Sr_{0.5}TiO_3$ powders prepared by sol–gel method were crystallized to the tetragonal phase after sintering at 750 °C for 1 h with the Curie temperature for the resulting ceramics to be only 75 °C [27]. No such reports are available for BTS prepared from nanopowders.

There are varieties of routes for the synthesis of nanoceramic powders such as chemical coprecipitation [28], sol–gel technique [29], hydrothermal synthesis [30]. However, the high-energy ball milling technique is still considered as a simple and cost effective method for large scale production of nanoceramic powders [31,32].

We prepared nanosized BST powders and ceramics with different proportions of Sn using the solid-state reaction process followed by high-energy ball milling. The influence of Sn content on the electrical and piezoelectric properties of $Ba(Ti_{1-x}Sn_x)O_3$ solid solution with $0 \le x \le 0.065$ was examined.

2. Experimental

Samples of $Ba(Ti_{1-x}Sn_x)O_3$ nanocrystalline powders, where $x = 0$, 0.025, 0.045 and 0.065, were synthesized by solid state reaction followed by high-energy ball milling. The raw materials were AR grade $BaCO_3$ (99.9%), TiO_2 (99.9%) and SnO_2 (99.8%). The raw materials were weighed in proportion to the stoichiometric ratio and then homogeneously mixed in isopropyl alcohol medium using ball mill with zirconia balls. The mixture was dried in an oven and calcined at 1050 °C for 4 h to yield $Ba(Ti_{1-x}Sn_x)O_3$. The calcined powders were then high-energy milled using planetary ball mill (Retsch PM100) in which the sun wheel and grinding jar rotate in opposite directions with speed ratio 1:−2. Agate vial and balls were used. The milling was performed at the angular speed of 200 rpm for 8 h. During each high-energy milling, a mass ratio of 1:5 for powder and balls was always maintained. The planetary ball mill was set to a rotational mode that changes the rotational direction of the vial and the sun wheel every 6 min after a rest interval of 2 min.

The particle sizes of the milled powders were examined by using TEM (Morgagni 268D). The milled powder was pressed into pellets of 10 mm diameter and 1 mm thickness under 2 MPa using polyvinyl alcohol (PVA) as a binder. After burning off PVA, the pellets were sintered at 1350 °C for 4 h in closed alumina crucible. The bulk density of the sintered specimens was measured using Archimedes principle. X-ray Diffractometer (Philips Diffractometer PW 3020) with monochromatic CuKα radiation ($\lambda = 1.54178$ Å) was used over a 2θ angle from 20° to 80° to characterize the crystalline phase of the sintered compacts. The microstructures of the polished surfaces were studied using SEM (Leo 1430, Japan). For the electrical measurements, silver paste was coated on both sides of the sintered samples and fired at 300 °C for 1 h to form electrodes. The temperature dependence of dielectric properties was measured with an impedance analyzer (Agilent 4294A) in an automated temperature-controlled furnace, which was interfaced with a computer for data acquisition. The polarization versus electric field (P–E) hysteresis loops of the ceramics were recorded using an automated P–E loop tracer (AR Imagetronics, India) operating at 50 Hz. For imparting the piezoelectric properties to the ceramics, the samples were poled at temperatures which are 15 °C lower than their Curie temperatures, in stirred silicone oil at 3 kV/mm for 30 min using a DC power supply, and then cooled to room temperature with the electric field. The planar electromechanical coupling factor (k_p) was calculated from the resonance–antiresonance frequencies recorded by the impedance analyzer. The field induced strain was measured using a SS50 strain measurement system (Sensor Tec Canada) with linear voltage differential transducer (LVDT) as displacement sensor and high voltage power supply (4 kV). The piezoelectric charge coefficient (d_{33}) was measured with a piezometer (Take Control, PM 25).

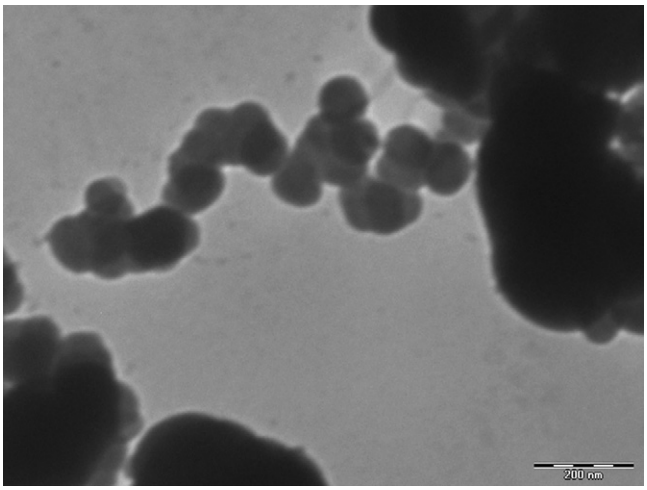

Fig. 1. Typical TEM micrograph of the milled powder of $Ba(Ti_{1-x}Sn_x)O_3$ system.

3. Result and discussion

Fig. 1 shows a typical TEM micrograph of nanocrystalline $Ba(Ti_{1-x}Sn_x)O_3$ powder prepared with planetary ball milling. The micrograph reveals that the powder particles are spherical in shape with an average particle size of ~86 nm.

Fig. 2 shows the room temperature X-ray diffraction patterns of $Ba(Ti_{1-x}Sn_x)O_3$ ceramics with $x = 0$, 0.025, 0.045 and 0.065. It is seen that all the compositions are of single phase perovskite structure. No trace of any secondary phase is detected.

The enlarged XRD patterns of the ceramics in the range of 2θ from 44° to 47° clearly show that the crystal structure of the ceramic is tetragonal for $x = 0$ and 0.025 and orthorhombic for $x = 0.045$ and 0.065, with the splitting of the (2 0 0) and (0 0 2) characteristic peaks at a 2θ of ~45.5° [33–37]. Moreover, it is noted that the positions of the diffraction peaks of the ceramics shift slightly to lower angles with increasing x. This result is attributed to the greater ionic radius of Sn^+(83.0 pm) as compared with that of Ti^+(74.5 pm), which gives rise to a small enlargement of cell volumes.

Fig. 3 shows the SEM micrographs of the polished surfaces of the ceramics sintered at the optimum sintering temperature of 1350 °C. The SEM results reveal that the average values of grain size of all the ceramics are about 0.2 μm. Such values of grain size are much smaller than those observed in traditional BT ceramics sin-

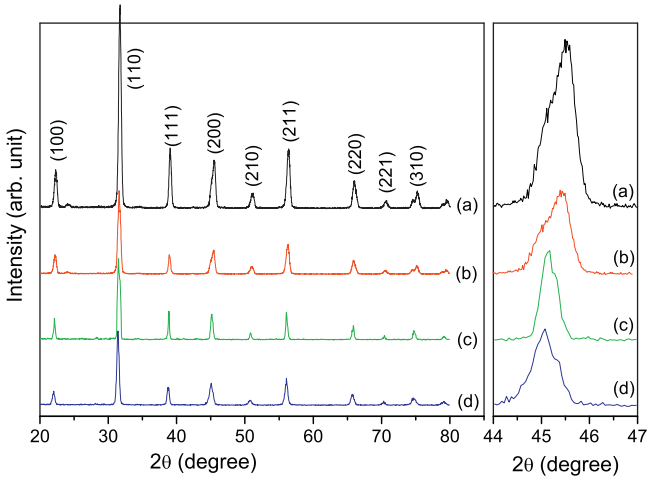

Fig. 2. XRD patterns of $Ba(Ti_{1-x}Sn_x)O_3$ ceramics with (a) $x = 0$, (b) $x = 0.025$, (c) $x = 0.045$, and (d) $x = 0.065$.

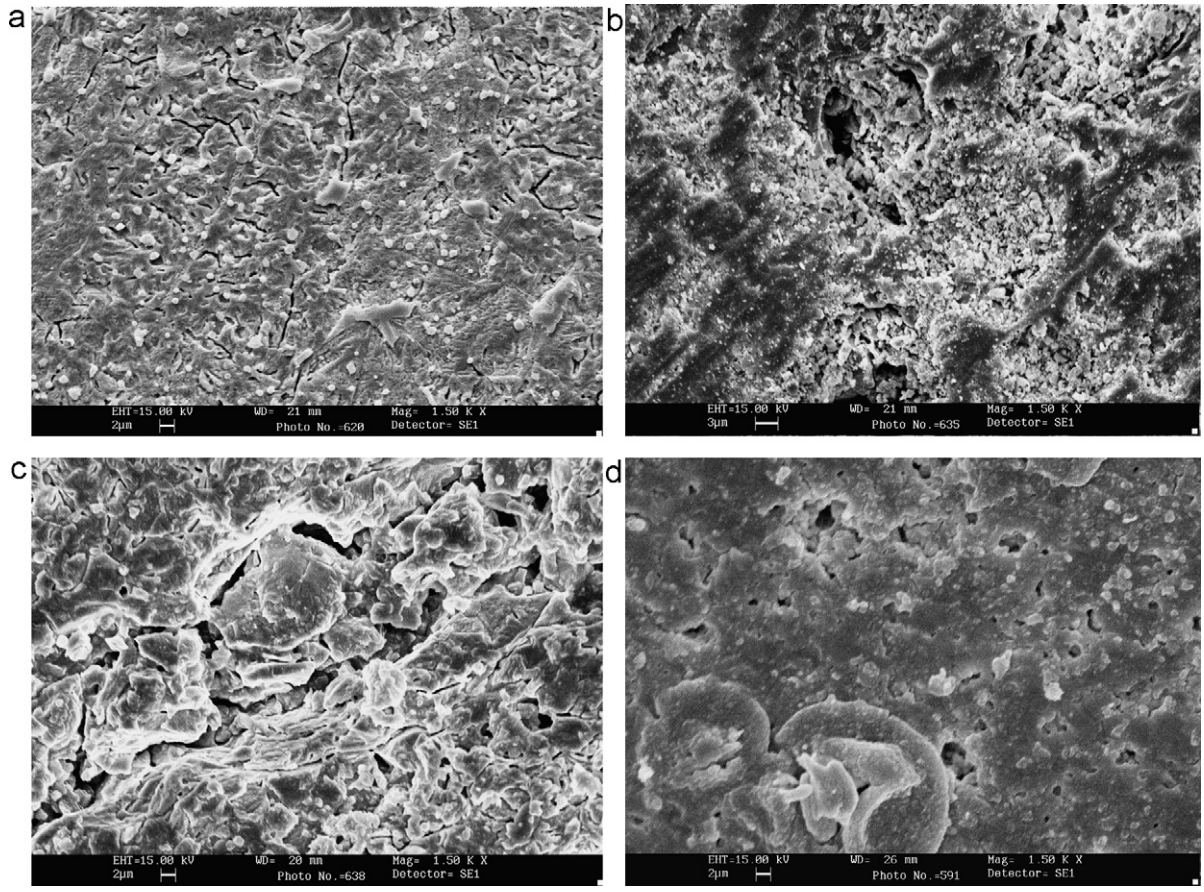

Fig. 3. SEM micrographs of $Ba(Ti_{1-x}Sn_x)O_3$ ceramics with (a) $x = 0$, (b) $x = 0.025$, (c) $x = 0.045$, and (d) $x = 0.065$.

tered at about 1450 °C. The small values of grain size are achieved due to the reduced optimum sintering temperature of the ceramics necessitated by the starting nanopowders. Grain growth and density decrease have been reported in such BTS ceramics with the increase of Sn concentration [38]. The present SEM micrographs also show a slight increase in the grain size of the ceramic samples as the Sn content increases. The observed decreasing trend in density values (Table 1) with increasing Sn concentration supports the existence of such grain growth, and perhaps an increase in porosity in the ceramic samples.

The apparent grain growth in BST ceramics with increasing Sn concentration may be understood in the following way. The grain growth behavior is a compromise between the driving force for movement of the grain boundary and retarding force created by the pores. In the present case, even if the high-energy ball milling can yield nanoscale powders with high sintering activity, excess SnO_2 accumulates near the grain boundaries forming oxides with a low melting point. The presence of these oxides enhances the mobility of grain boundaries as densification occurs. The increase in the mobility of the grain boundaries promotes the mass transportation and thereby the grain growth.

Table 1
Various observed properties of $Ba(Ti_{1-x}Sn_x)O_3$ ceramics.

Parameter	$x = 0$	$x = 0.025$	$x = 0.045$	$x = 0.065$
Density (g/cm^3)	5.84	5.55	5.43	5.20
T_c (°C)	115	104	75	45
ε' (100 kHz, 25 °C)	1524	1238	1702	1126
ε'_m (100 kHz)	7139	2415	2034	1220
γ	1.23	1.61	1.66	1.71
P_r (μC/cm^2)	5.2	3.1	1.8	0.3
E_c (kV/cm)	4.6	2.5	1.6	0.8
Strain (%)	0.097	0.084	0.059	0.027
k_p (%)	41.2	33.6	27.4	19.3
d_{33} (pC/N)	183	111	60	4

Fig. 4 shows the temperature dependence of the dielectric constant ε' and dielectric loss ($\tan\delta$) of $Ba(Ti_{1-x}Sn_x)O_3$ ceramic samples with $x = 0$, 0.025, 0.045 and 0.065, measured at 100 kHz from room temperature up to 150 °C. The ε'–T curves of the ceramic samples with $x = 0$, 0.025, 0.045 and 0.065 exhibit one peak corresponding to the ferroelectric to paraelectric phase transition (at 45 °C ~ 115 °C, T_c).

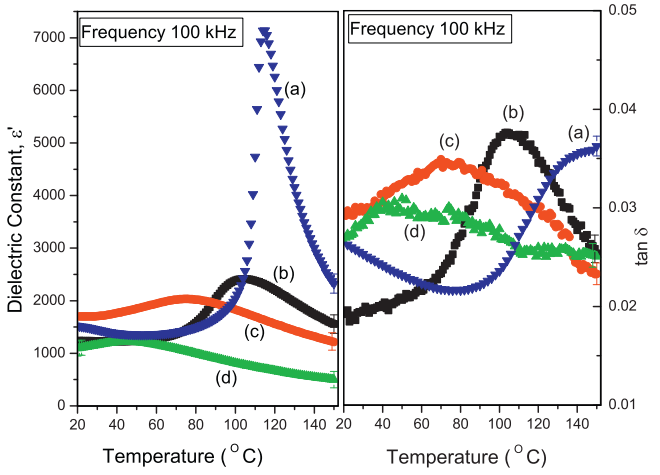

Fig. 4. Temperature dependence of ε' for $Ba(Ti_{1-x}Sn_x)O_3$ ceramics with (a) $x = 0$, (b) $x = 0.025$, (c) $x = 0.045$, and (d) $x = 0.065$, measured at 100 kHz.

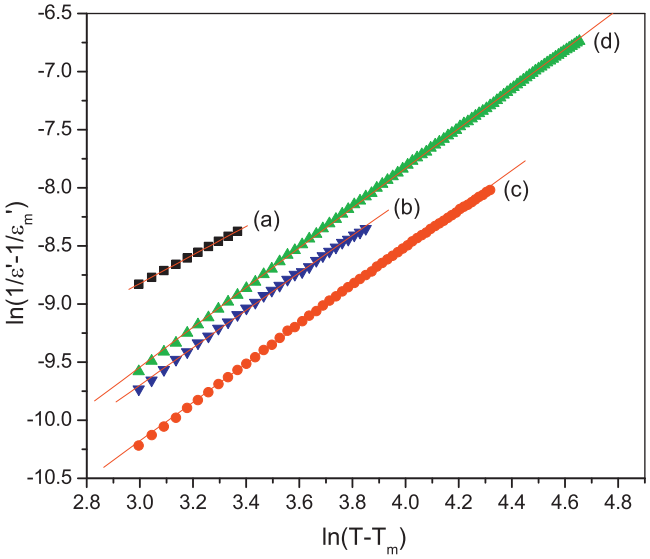

Fig. 5. Plots of $\log(1/\varepsilon'-1/\varepsilon_{m'})$ versus $\log(T-T_m)$ for $Ba(Ti_{1-x}Sn_x)O_3$ ceramics with (a) $x=0$, (b) $x=0.025$, (c) $x=0.045$, and (d) $x=0.065$.

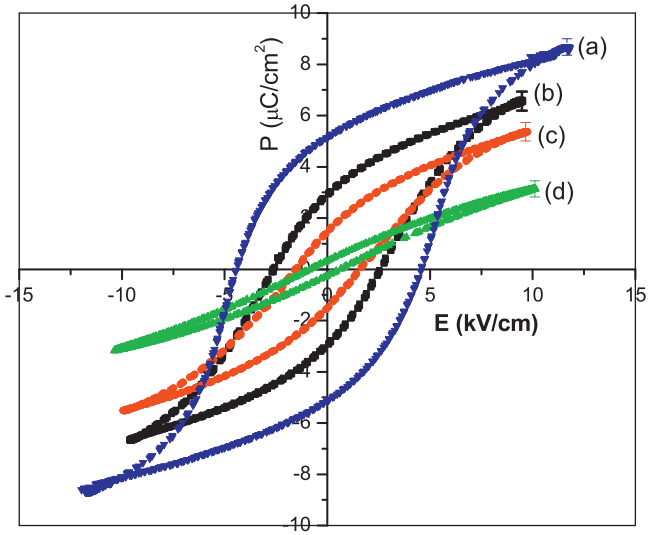

Fig. 6. *P–E* hysteresis curves of $Ba(Ti_{1-x}Sn_x)O_3$ ceramics with (a) $x=0$, (b) $x=0.025$, (c) $x=0.045$, and (d) $x=0.065$, measured at 25 °C and 50 Hz.

It is seen in Fig. 4 that with increasing Sn concentration, the T_c shifts gradually towards lower temperature and there is a systematic broadening of peak in dielectric constant at T_c. The shifting of transition temperature (T_c) to a lower value can be explained by the larger radius of Sn^{4+} (83.0 pm) compared to Ti^{4+} (74.5 pm) and the fact that Sn^{4+} occupies sites formerly occupied by Ti^{4+}. The Sn^{4+} is distributed uniformly in the $BaTiO_3$ and forms a $Ba(Ti_{1-x}Sn_x)O_3$ solid solution which makes the partial crystal cell take on center symmetry at room temperature. The nonferroelectric barium stannate dilutes the ferroelectricity of barium titannate and thus makes the spontaneous polarization less stable. The result is that the phase transition temperature of barium stannate titanate ceramics shifts progressively towards a lower temperature. Uchino et al. suggested that with decreasing grain size, T_c was shifted downward through room temperature, eventually tending toward 0 K at some critical particle size [39]. In the present study, with the grain size of ~0.2 μm, the lowering of T_c observed may be due to both the increase in Sn concentration and the smallness of the grain size.

The broadening of the dielectric peak can be attributed to the coalescence of the low temperature phase transformations such as the transformation from rhombohedral to orthorhombic and from orthorhombic to tetragonal [40]. The diffuseness of the phase transition was analyzed using the modified Curie–Weiss law, proposed by Uchino and Nomura [41]:

$$\frac{1}{\varepsilon'}-\frac{1}{\varepsilon'}=\frac{(T-T_m)^{\gamma}}{C_1},\ (T>T_m) \quad (1)$$

where γ and C_1 are modified constants, with $1<\gamma<2$. The value of γ determines the degree of diffuseness of the phase transition. The value of γ is equal to 1 for a system with a completely ordered transition. On the basis of a local compositional fluctuation model, the value of γ is equal to 2 for a completely diffuse system.

The plots of $\log[(1/\varepsilon')-(1/\varepsilon_{m'})]$ versus $\log(T-T_m)$ corresponding to the samples for $x=0$, 0.025, 0.045 and 0.065, are shown in Fig. 5. According to Eq. (1), the slope of the $\log[(1/\varepsilon')-(1/\varepsilon_{m'})]$ versus $\log(T-T_m)$ plot gives the value of γ. The values of γ calculated from the curve fitting of the graphs in Fig. 5 are given in Table 1. It can be noted that γ increases from 1.23 to 1.71 indicating that the ferroelectric transition becomes more diffuse as Sn content increases from $x=0$ to 0.065.

It can be noted from Fig. 4 that the value of dielectric loss ($\tan\delta$) remains below 0.04 for all the ceramic samples over the range of temperature studied.

The values of dielectric constant (ε') at 100 kHz and 25 °C for various Sn contents are shown in Table 1. As shown in Table 1, the maximum dielectric constant ε'_m of the ceramics for $x=0$ at T_c has a value of only 7139. This value is very small for the BT ceramics. The observed lower value in ε'_m may be due to the smaller grain size of the ceramics. As the crystallite size reduces and becomes comparable to the width of the domain wall, pinning would be developed inside the grains and the domain-wall motion would be inhibited. The reduction in the domain wall mobility would decrease the switching rate, thereby lowering ε'_m. The presence of Sn in the ceramics also decreases the maximum dielectric constant of BST [15]. The observed lowering of ε'_m for $x=0.025$ to 0.065 could be considered as a combined effect of the presence of Sn and the nanocrystalline nature of the grains.

Fig. 6 shows the *P–E* hysteresis loops measured at room temperature of BTS ceramics with various Sn concentrations. Well saturated hysteresis shape typical of ferroelectric materials is evident for the ceramics with $x=0$, 0.025, 0.045 and 0.065. The *P–E* loops become narrower as the content of Sn increases. The values of remnant polarization (P_r) and coercive field (E_c), determined from the loops are summarized in Table 1. It is seen that P_r and E_c values follow a decreasing trend with increasing concentration of Sn.

The profiles of *P* vs *E* curves are clearly related to the crystalline structure of the samples at room temperature. For BTS samples having room temperature ferroelectric tetragonal phase ($x=0$ and 0.025) and ferroelectric orthorhombic phase ($x=0.045$ and 0.065) as evident from XRD results in Fig. 2, saturated polarization loops are obtained. BTS is a binary solid solution composed of ferroelectric barium titanate and non ferroelectric barium stannate [12]. The partial substitution of Ti^{4+} ion in $BaTiO_3$ by Sn^{4+} ion results in shifting the ferroelectric–paraelectric transition (T_c) to lower temperatures, as observed in the dielectric results of Fig. 4. As a consequence to the shifting of T_c, the ferroelectric property of BTS degrades with the increase of Sn content and P_r reduces gradually from 5.2 μC/cm² for $x=0$ to 0.3 μC/cm² for $x=0.065$. As shown in Fig. 4, at $x=0.065$, the paraelectric cubic phase has approached so close to the room temperature (Fig. 4), the temperature of our *P–E* measurement, as to dilute the ferroelectric property of the BTS sample as observed in Fig. 6.

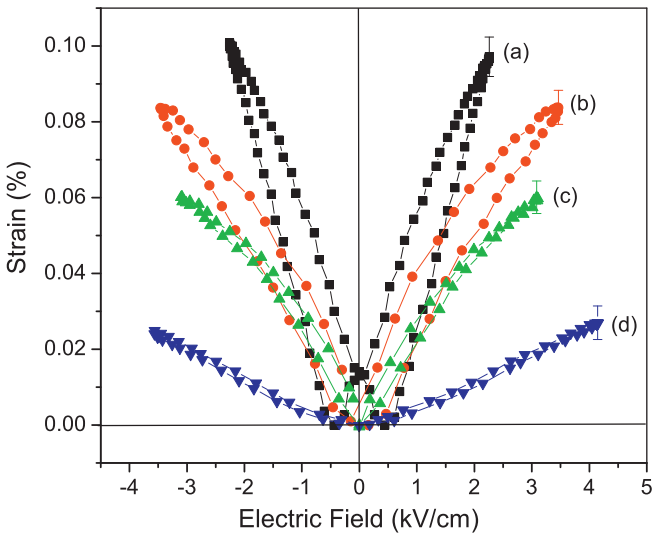

Fig. 7. Strain vs electric field curves of $Ba(Ti_{1-x}Sn_x)O_3$ ceramics with (a) $x = 0$, (b) $x = 0.025$, (c) $x = 0.045$, and (d) $x = 0.065$.

The bipolar strain (S) versus electric filed (E) hysteresis loops for $Ba(Ti_{1-x}Sn_x)O_3$ ceramics is shown in Fig. 7. The hysteretic strain could be associated with the domain reorientation in the samples. It can be seen in Fig. 7 that the bipolar strain level decreases gradually with increasing Sn concentration from 0.097% for $x = 0$ to 0.027% for $x = 0.065$. The strain values are given in Table 1. Compared with other samples, the sample with $x = 0.045$ exhibits a reasonably high strain level of 0.059% with proportionately small hysteresis loop area, a property desirable for application in positioning actuators. The observed S vs E profile for $x = 0.065$ is due to a mixed state including local polarization contribution originated from the ferroelectric-relaxor behavior, in addition to the electrostrictive effect of paraelectric state.

The values of electromechanical coupling coefficient (k_p) of $Ba(Ti_{1-x}Sn_x)O_3$ ceramics measured by the resonance–antiresonace method are presented in Table 1. The value of k_p is seen to gradually decrease from 41.2%, which is reasonably high for the lead-free BT ceramics, to 19.3% as the Sn concentration increases from $x = 0$ to 0.065.

The piezoelectric charge constant (d_{33}) observed for the ceramic samples vary in the range of 183–4 pC/N. The observed value of $d_{33} = 183$ pC/N is close to the maximum reported value of ~190 pC/N [42] for BT ceramics fabricated by conventional sintering using chemical powder prepared from $BaCO_2$ and TiO_2. Wada et al. [43] reported that with decreasing grain size, domain size decreases and hence piezoelectric properties of the ceramics increase. However, for the present grain size, no significantly high d_{33} value is observed. This may be due to the fact that the present grain size (~0.2 μm) is so small that other mechanisms like pinning of domain walls set in to disrupt the further improvement in piezoelectric behavior with decreasing grain size. The observed lower value of d_{33} thus supports the existence of an appropriate grain size, 3.1–3.4 μm, for better piezoelectric properties [44] in BT. This viewpoint is also in agreement with the lower dielectric constant observed for the present grain size as discussed earlier. The decrease in piezoelectric properties of the ceramic samples with increase in Sn concentration, shown in Table 1, can be attributed to the associated decrease in the density and degradation of ferroelectricity with lower P_r.

4. Conclusions

Nanocrystalline $Ba(Ti_{1-x}Sn_x)O_3$ powders with $x = 0$, 0.025, 0.045 and 0.065, having average particle size of 86 nm, were prepared by solid state reaction accompanied by high energy ball milling. As the Sn content increases in the ceramic, the Curie temperature (T_c) progressively shifts towards the lower temperature while the phase transition becomes more diffuse. Increasing Sn concentration produces decrease in remnant polarization (P_r) and coercive field (E_c). The unipolar strain level of ~0.097% for $x = 0$ gradually decreases to ~0.027% for $x = 0.065$. The values of electromechanical coupling factor k_p and the piezoelectric charge constant d_{33} determined for the ceramics with $x = 0$ are high at 41.2% and 183 pC/N respectively. These values gradually decreases to 19.3% and 4 pC/N respectively as the Sn content in the ceramics increases.

Acknowledgements

The financial support from UGC of India in form of Major Research Project Scheme vide No. F. 33-25/2007(SR) is gratefully acknowledged. We also acknowledge the Directors, Solid State Physics Laboratory and AIIMS, Delhi, for providing facilities for some measurements.

References

[1] Z. Yu, R. Guo, A.S. Bhalla, J. Appl. Phys. 88 (2000) 410–415.
[2] J. Zhao, L. Li, Y. Wang, Z. Gui, Mater. Sci. Eng. B 99 (2003) 207–210.
[3] B.D. Stojanovic, C.R. Foschini, V.B. Pavlovic, V.M. Pavlovic, V. Pejivic, J.A. Varela, Ceram. Int. 28 (2002) 293–298.
[4] B. Cui, P.F. Yu, J. Tian, H.L. Guo, Z.G. Chang, Mater. Sci. Eng. A 454–455 (2007) 667–672.
[5] D. Voltzhe, H.P. Abicht, Solid State Sci. 2 (2000) 149–159.
[6] B. Cui, P.F. Yui, J. Tian, Z.G. Chang, Mater. Sci. Eng. B 139 (2006) 205–208.
[7] Y. Wang, B.T. Liu, F. Wei, Z.M. Yang, J. Du, J. Alloys Compd. 475 (1–2) (2009) 827–831.
[8] H.W. Chen, C.R. Yang, C.L. Fu, J. Shi, J. Zhang, W. Leng, J. Mater. Sci.: Mater. Electron. 19 (4) (2008) 379–382.
[9] W. Cai, C. Fu, J. Gao, X. Deng, J. Mater. Sci.: Mater. Electron. 21 (2010) 317–325.
[10] S.W. Zhang, H. Zhang, B.P. Zhang, S. Yang, J. Alloys Compd. 506 (1) (2010) 131–135.
[11] W. Xiaoyong, F. Yujun, Y. Xi, Appl. Phys. Lett. 83 (10) (2003) 2031–2033.
[12] S.G. Lu, Z.K. Xu, H. Chen, Appl. Phys. Lett. 85 (22) (2004) 5319–5321.
[13] X. Wei, X. Yao, Mater. Sci. Eng. B 137 (2007) 184–188.
[14] Y. Ishibashi, M. Iwata, J. Phys. Soc. Jpn. 65 (1996) 854–857.
[15] V.A. Isupov, Ferroelectr. 90 (1989) 113–118.
[16] H.H. Huang, M.C. Wang, C.Y. Chen, Mater. Sci. Eng. A 433 (2006) 279–285.
[17] W. Cai, Y. Fan, J. Gao, C. Fu and X. Deng, J Mater Sci: Mater. Electron., doi:10.1007/s10854-010r-r0126-7.
[18] S. Singh, P. Singh, O. Prabhakar, D. Parkash Kumar, J. Alloys Compd. 493 (1–2) (2010) 522–528.
[19] S. Wang, T.A. Tan, M.O. Lai, L. Lu, Mater. Res. Bull. 45 (3) (2010) 279–283.
[20] G. Aldica, M. Cernea, R. Radu, R. Trusca, J. Alloys Compd. 505 (1) (2010) 273–277.
[21] J. von Cieminski, H. Beige, J. Phys. D: Appl. Phys. 24 (1991) 1182–1186.
[22] L.B. Kong, T.S. Zhang, J. Ma, F. Boey, Prog. Mater. Sci. 53 (2008) 207–322.
[23] T. Karaki, K. Yan, T. Miyamoto, M. Adachi, Jpn. J. Appl. Phys. 46 (2007) L97–L98.
[24] K. Wu, W. Schltze, J. Am. Cer. Soc. 75 (1992) 3390–3395.
[25] M.H. Frey, D.A. Payne, Phys. Rev. B 54 (1996) 3158–3168.
[26] W. Li, Z. Xu, R. Chu, P. Fu, J. Hao, J. Alloys Compd. 499 (2) (2010) 255–258.
[27] R.M. Mahani, I.K. Battisha, M. Aly, A.B. Abou-Hamad, J. Alloys Compd. 508 (2) (2010) 354–358.
[28] M. Buscaglia, Z. Zhao, V. Buscaglia, M. Viviani, M.T. Buscaglia, L. Mitoseriu, Testino, Nanotechnol. 15 (2004) 1113–1117.
[29] J. Cho, M. Kubawara, J. Eur. Ceram. Soc. 24 (2004) 2959–2968.
[30] H. Xu, L. Gao, J. Guo, J. Eur. Ceram. Soc. 22 (2002) 1163–1170.
[31] T. Venugopal, K.P. Rao, B.S. Murty, J. Nanosci. Nanotechnol. 7 (2007) 2376–2381.
[32] Y. Wang, Y. Li, C. Rong, P. Liu, J. Nanotechnol. 18 (2007) 465701.
[33] D. Lin, K.W. Kwok, K.H. Lam, H.L.W. Chan, J. Appl. Phys. 101 (2007) 074111–74116.
[34] M. Matsubara, T. Yamaguchi, W. Sakamoto, K. Kikuta, T. Yogo, S. Hirano, J. Am. Ceram. Soc. 88 (5) (2005) 1190–1196.
[35] M. Matsubara, T. Yamaguchi, K. Kikuta, S. Hirano, Jpn. J. Appl. Phys. 44 (8) (2005) 6136–6142.
[36] N.M. Hagh, B. Jadidian, A. Safari, J. Electroceram. 18 (2007) 339–346.
[37] G.C. Jiao, H.Q. Fan, L.J. Liu, W. Wang, Mater. Lett. 61 (19–20) (2007) 4185–4187.
[38] F. Du, B. Cui, H. Cheng, R. Niu, Z. Chang, Mater. Res. Bull. 44 (2009) 1930–1934.
[39] K. Uchino, E. Sadanaga, T. Hirose, J. Am. Ceram. Soc. 72 (1989) 1555–1558.
[40] N. Yasuda, H. Ohwa, S. Asano, Jpn. J. Appl. Phys. 35 (1996) 5099–5103.
[41] K. Uchino, S. Nomura, Integr. Ferroelectr. 44 (1982) 55–61.
[42] R. Bechman, J. Acoust. Soc. Am. 28 (1956) 347–350.
[43] S. Wada, K. Yaku, H. Kakamoto, T. Tsurumi, J. Appl. Phys. 98 (2005) 014109.
[44] H. Takahashi, Y. Numamoto, J. Tani, K. Matsuta, J. Qiu, S. Tsurekawa, Jpn. J. Appl. Phys. 45 (2006) L30–L32.